Journal of Vacuum Science Technology A

Atomic layer deposition of GdF_3 thin films

Running title: Atomic layer deposition of GdF_3 thin films

Running Authors: Atosuo et al.

Elisa Atosuo [1, a)], Kenichiro Mizohata [2], Miika Mattinen [1, 3], Miia Mäntymäki [1], Marko Vehkamäki [1], Markku Leskelä [1] and Mikko Ritala [1]

[1]Department of Chemistry, University of Helsinki, P.O. Box 55, FI-00014 Helsinki, Finland
[2]Department of Physics, University of Helsinki, P.O. Box 43, FI-00014 Helsinki, Finland
[3]Present address: Department of Applied Physics, Eindhoven University of Technology, P.O. Box 513, 5600 MB Eindhoven, The Netherlands

[a)] Electronic mail: elisa.atosuo@helsinki.fi
mikko.ritala@helsinki.fi

ABSTRACT

Gadolinium fluoride is an attractive optical material with applications in e.g. deep-UV lithography, solar cells and medical imaging. Despite the interest towards this material, no atomic layer deposition (ALD) process has been published. In this article, an ALD process for GdF_3 using $Gd(thd)_3$ and NH_4F as precursors is presented. The deposition was studied at temperatures 275–375 °C, but 285–375 °C produce the purest films. The saturation of the growth per cycle (GPC) with respect to precursor pulses and purges was proved at 300 °C. The GPC value at this temperature is ~0.26 Å, and the deposition temperature has very little effect on the GPC. According to X-ray diffraction (XRD), all the films consist of orthorhombic GdF_3. The impurity contents, evaluated by time-of-flight elastic recoil detection analysis (ToF-ERDA), are low and the films are close to stoichiometric. The nitrogen content is less than <0.04 at-%. The antireflection properties

were qualitatively evaluated by UV-vis spectrometry in transmission mode at 190−1100 nm range: on sapphire substrates, GdF_3 serves as an antireflective coating. Dielectric properties of the films were studied and for example permittivity value of 9.3 was measured for ~64 nm film deposited at 300 °C.

I. INTRODUCTION

Photolithography is one of the critical steps in the miniaturization of microelectronic devices. As an example, the advances in deep-UV (DUV) lithography since the 1990s have decreased the feature sizes remarkably. There is pressure to decrease the feature size further, and the technology for extreme-UV (EUV) lithography already exists. However, the cost of the EUV method has limited its use thus far, and therefore the deep-UV lithography remains the market-dominating photolithography method.[1]

An important part of a deep-UV photolithography machine are the narrow-band filters. For these, antireflection coatings of low and medium refractive index are needed. GdF_3 and LaF_3 are among the few materials that fulfil the requirements for the medium refractive index material: high transparency and low loss.[2, 3] LaF_3 already has an atomic layer deposition (ALD) process, whereas GdF_3 has been lacking one.[4] Motivated by this, an ALD process for GdF_3 was developed in this work.

Another important application for GdF_3 is likewise in the field of optics: in applications utilizing luminescence. But unlike several rare earth metals, gadolinium has a role in host materials for luminescence centers rather than as the luminescence centers themselves. Due to the half-filled 4f shell, Gd^{3+} lacks the characteristic, visible-light

range, 4f-4f transitions of other rare earth ions. Instead, after high-energy absorption, it emits at UV range and can transfer the energy to the active luminescent ions, e.g., other rare earth ions embedded in the host structure. In the host structures, gadolinium is often present as a fluoride, since fluorides are unlikely to cause non-radiative decay of the excited states due to low phonon energies.[5, 6]

GdF_3 and related materials, such as $NaGdF_4$ and $KGdF_4$, have been studied as host materials especially for up-converting and down-converting luminescence systems.[7] In up-conversion, two or more photons are converted to a photon of higher energy, whereas in down-conversion, the opposite occurs. The main target of the research has been in medical applications[8] —both imaging and therapy — but the conversion properties can be exploited also in solar cells. The part of the solar spectrum that can be exploited is limited by the band gap of the absorber, but it can be widened by up-converting low energy photons.[9] High-energy photons, which otherwise would be eventually lost as heat, can be down-converted to energy ranges suitable for electron-hole production.[10]

GdF_3-based materials have attracted interest as optical thermometers in recent years. The use of rare earth-based materials as thermometers relies on the temperature sensitivity of the luminescence. For example, in Sr_2GdF_7 doped with Yb^{3+} and Er^{3+}, even a small change in temperature gives rise to a different intensity ratio of two green emission bands of Er^{3+}.[Ref. 11] This enables accurate measurements, and due to non-contact operation, also working in harsh conditions. Yet another application field for rare earth-based luminescence is anti-counterfeiting. Here one exploits the unique luminescence fingerprint formed upon mixing different rare earth ions. These mixtures

are an excellent choice for e.g. hard-to-replicate security inks.[12] Also in these applications, GdF_3 is a potential host material.[13] Although the main applications of GdF_3 and GdF_3-based materials are related to optics, GdF_3 has also been studied for thin film capacitor applications[14] owing to its high band gap of ~10 eV.[Ref. 15]

Current GdF_3 thin film synthesis methods include several physical vapor deposition (PVD) methods, e.g., thermal evaporation and electron beam evaporation. Of chemical deposition methods, only a metal organic chemical vapor deposition (MOCVD) process has been reported.[16] All but MOCVD are so called line-of-sight methods, i.e., the film is deposited uniformly only on flat surfaces. The advantage of the ALD method is the ability to coat uniformly also surfaces with complicated morphologies, such as cavities, curved surfaces and even nanoparticles. In ALD, alternately supplied gaseous precursors react in a self-limiting manner on the substrate surface. As a result, a uniform coating is obtained, together with the ability to precisely control the thickness of the coating by adjusting the number of precursor pulse cycles. This is especially useful in applications where stacks of thin layers are needed, e.g., in narrow-band filters. Due to the self-limiting nature, ALD is also highly reproducible. More on the basics of the method can be found in Ref. 17.

In ALD of several metal fluorides, including rare earth fluorides YF_3, LaF_3, and TbF_3, titanium tetrafluoride and tantalum pentafluoride have been used as the fluorine precursor.[4, 18–29] However, the use of these metal fluorides often introduces titanium or tantalum impurities into the films. The presence of these impurities increases the absorption of UV light, and thus leads to a loss of the desired optical properties.

The most intuitive choice for a fluorine source other than TiF_4 or TaF_5 is HF. It has been used as a precursor in ALD, but the toxic and hazardous nature has limited its use. Ammonium fluoride as a safer option for pure HF was introduced by Ylilammi et al. already in 1994.[Ref. 30] The use of NH_4F is based on its in-situ decomposition into NH_3 and HF at elevated temperatures. Recently, renewed interest has been shown towards this precursor, as it has been used in ALD of rare earth fluorides and LiF.[Refs. 31, 32] In this work, NH_4F was combined with $Gd(thd)_3$ to produce GdF_3 thin films.

II. EXPERIMENTAL

A. Film deposition

All the depositions were done in a F120 cross-flow ALD reactor (ASM Microchemistry Ltd.) using nitrogen (99.995%) as carrier and purging gas. The sublimation temperatures for $Gd(thd)_3$ (Strem chemicals) and NH_4F (Sigma-Aldrich, ≥99.99%) were 135 °C and 65 °C. Both precursors were delivered from glass boats inside the reactor using inert gas valving. Most of the films were deposited on Si(100) substrates with a native oxide. The silicon substrates were used as received and were only blown with a stream of nitrogen to remove particles. 2'' double-side polished c-plane (0001) sapphire substrates (University wafers) were used as substrates for UV-Vis transmittance measurements and indium tin oxide (ITO) coated glass substrates were used for electrical measurements.

B. Film characterization

The thicknesses and refractive indices of the films were measured by Film Sense FS-1 Multi-wavelength ellipsometer and the data was fitted with Cauchy model.

Some of the thicker films were measured with a Hitachi U2000 spectrophotometer in reflectance mode and fitted with the program of Ylilammi and Ranta-aho[33]. Film densities were evaluated with PANalytical X'pert Pro MPD diffractometer in x-ray reflectivity mode (XRR). The same diffractometer in x-ray diffraction mode (XRD) was used for crystallinity determinations. The radiation source was Cu K_α and the measurements were done in grazing incidence mode. Crystalline phases were identified with PANalytical HighScore plus software (version 4.7). For morphology determination, Hitachi S-4800 field-emission scanning electron microscope (FESEM) was used. The samples were coated with Au/Pd alloy to increase the conductivity. Further morphology studies were done by atomic force microscope (AFM) using a Veeco Multimode V instrument in tapping mode. Images were captured in air using silicon probes with a nominal tip radius of 10 nm and a nominal spring constant of 5 N/m (Tap150 from Bruker). Images were flattened to remove artefacts caused by scanner bow and sample tilt. Roughness was calculated as a root-mean-square value (R_q).

The stoichiometry and the impurity contents of the films were determined with time-of-flight elastic recoil detection analysis (ToF-ERDA) utilizing a 5 MV tandem accelerator at the accelerator laboratory of University of Helsinki. Measurements were performed using 35–40 MeV ^{79}Br or ^{127}I primary ions and 40° detection angle. UV-Vis transmission spectra of the films were measured with a Hitachi U2000 spectrophotometer in a wavelength range of 190–1100 nm.

For dielectric measurements, capacitors were made by growing GdF_3 films on indium tin oxide (ITO) films on glass substrates, followed by electron beam evaporation of aluminum top electrodes through a shadow mask. The capacitance was measured with

an HP 4282A LCR meter, using a 10 kHz measurement frequency. I-V measurements were performed with a Keithley 2450 SourceMeter instrument.

Film adhesion to the Si-substrate was tested with the Scotch tape test.

III. RESULTS AND DISCUSSION

A. Film growth

The most important requirement for an ALD process is the self-limiting growth mode. For this process, the saturation of the growth per cycle (GPC) with respect to precursor pulse lengths and purge lengths was verified at 300 °C. Fig. 1a depicts the GPC of GdF_3 as a function of $Gd(thd)_3$ pulse length. The NH_4F pulses and both purges were 1 s. As is seen in the figure, the GPC reaches saturation already with 0.5 s pulses, resulting in a GPC value of ~0.23 Å.

The saturation of the GPC with respect to NH_4F pulse was studied while keeping the $Gd(thd)_3$ pulse at 0.5 s and the purges at 1 s. As seen in Fig. 1b (squares), 3 s NH_4F pulses is needed to reach saturation, and the GPC value is ~0.26 Å. The effect of purge time was investigated by increasing the purge lengths to 2 s (Fig. 1b, crosses). The GPC is almost the same as that observed with 1 s purges, and hence 1 s purges are considered sufficient. Because both precursors were delivered from solid sources and the consumption of NH_4F was higher, the flux of HF appears to be higher than that of $Gd(thd)_3$. Therefore, the longer pulse time needed for NH_4F seems to be due to kinetic reasons, i.e., reactions during the NH_4F pulse require more time to be completed.

FIG. 1. GPC as a function of a) $Gd(thd)_3$ pulse length and b) NH_4F pulse length (squares) and purge length (crosses) at deposition temperature of 300 °C with 1000 cycles.

The dependence of the GPC on the cycle number was studied at the same deposition temperature. As depicted in Fig. 2, the thickness of the film grows linearly with increasing cycle number. However, according to the line fitting, the thickness of the film would be 36 Å when zero cycles is applied. Thus, in the beginning of the growth process, the GPC may be higher compared to later growth stages. This may indicate a surface enhanced growth mode.

FIG. 2. Thickness of GdF_3 films as a function of ALD cycles at 300 °C.

The GPC as a function of the deposition temperature was studied between 275 and 375 °C. The lower limit for the deposition temperature is dictated by the increase of impurities in the films, as will be discussed later. Higher deposition temperatures, in turn, were not studied as they lead to increasing roughness of the films and hence to light scattering losses. In addition, we wanted to avoid exposing the reactor parts made of glass and quartz to HF at high temperatures.

Fig. 3 illustrates the GPC as a function of the deposition temperature. In the studied temperature range, the GPC increases only slightly with increasing temperature, from 0.22 to 0.26 Å/cycle. However, the saturation of the GPC was studied only at 300

°C, and therefore the GPC values given for the other deposition temperatures are not necessarily exact. Although Niinistö et al. observed $Gd(thd)_3$ decomposition at 350 °C[Ref. 34], no clear sign of decomposition, i.e., a sudden rise of the GPC, was observed in the deposition temperature study.

In general, the GPC of the current process is lower compared to the ALD metal fluoride processes using TiF_4 as the fluorine source. In these processes, exceptionally high GPC (e.g. 5.2 Å at 250 °C in Ref. 4) has been reported. In addition, the almost temperature independent GPC in the current process is in striking contrast to the TiF_4-based ALD processes, where the GPC decreases strongly as the deposition temperature is increased.[4, 18–21, 23, 25] From the viewpoint of process control, the nearly temperature-independent GPC of the current process is an advantage.

FIG 3. GPC as a function of deposition temperature for 4000 cycle films.

B. Film properties

The crystallinity of the films as well as the crystalline phases were studied with grazing incidence (GI) XRD. Fig. 4 presents the x-ray diffractograms of films deposited with 4000 cycles at 275–375 °C and a 1000 cycle film deposited at 275 °C. All the measured films are crystalline and consist of orthorhombic GdF_3.[Ref. 35] In addition to the reflections belonging to GdF_3, in some cases, a reflection at a 2θ angle of 29° is seen in the film deposited at the lowest deposition temperature. The additional reflection is likely to originate from the cubic Gd_2O_3 phase, which has the strongest reflection at a 2θ angle of 28.6°.[Ref. 36]

To investigate, what is the lowest deposition temperature where the additional reflection is not seen, several films were deposited at temperatures between 275 and 300 °C with 5 °C intervals. 285 °C was found to be the lowest deposition temperature that provides XRD phase pure GdF_3 films.

FIG. 4. GI-x-ray diffractograms of 4000 cycle films deposited at 275–300 °C and a 1000 cycle film deposited at 275 °C.

The stoichiometry and impurities of the films were measured with ToF-ERDA. During the ERDA-measurement the films erode which is occasionally observed with fluoride films.[19, 25] Therefore, the data was collected in time dependent mode, allowing us to follow desorption of elements and other changes during the measurement. In the cases where changes were noted, the original sample compositions were obtained by extrapolating the data to zero beam fluence.

Table 1 lists the measured impurity contents and the F/Gd ratios of approximately 100 nm films deposited at 285–375 °C. These contents are averaged through the whole film including surface and Si/GdF_3 interface regions.

In all the films, low contents of H, C, and O were detected. The content of C is the lowest, ranging from 0.07 to 0.23 at-%. The H content is in maximum 0.5 at-%. The main impurity is oxygen, but only in the film deposited at the lowest temperature the oxygen content is higher than 1 at-%. In the films deposited at 285, 350, and 375 °C, also small content of nitrogen was detected with the estimated values of <0.03, <0.04, and <0.02 at-

%, respectively. The low nitrogen content verifies that NH_3 released from NH_4F is not participating in the reactions.

The F/Gd ratio is less than 3.0 in the film deposited at 285, 350, and 375 °C, being 2.9, 2.7, and 2.8, respectively. The films deposited at 300 and 325 °C are in turn fluorine rich, having F/Gd ratios of 3.3 and 3.2. In general, the low impurity content across the deposition temperature range indicates that no remarkable $Gd(thd)_3$ decomposition is occurring. This conclusion is in line with the GPC results (Fig. 3).

TABLE I. Impurity content and stoichiometry of approximately 100 nm thick films deposited at 285–375 °C as measured by ToF-ERDA.

Deposition temperature (°C)	Gd (at-%)	F (at-%)	H (at-%)	C (at-%)	N (at-%)	O (at-%)	F/Gd
285	25.55 ± 0.14	72.8 ± 0.6	0.38 ± 0.09	0.17 ± 0.02	<0.03	1.03 ± 0.07	2.9
300	23.2 ± 0.2	76.1 ± 0.7	0.27 ± 0.10	0.08 ± 0.01	-	0.31 ± 0.05	3.3
325	23.8 ± 0.2	75.4 ± 0.6	0.20 ± 0.07	0.07 ± 0.01	-	0.56 ± 0.08	3.2
350	26.56 ± 0.14	72.1 ± 0.6	0.5 ± 0.2	0.23 ± 0.04	<0.04	0.60 ± 0.04	2.7
375	26.20 ± 0.13	72.5 ± 0.6	0.38 ± 0.14	<0.12	<0.02	0.81 ± 0.05	2.8

During our previous fluoride deposition experiments with NH_4F, Si incorporation into the films was suspected (unpublished results). The HF formed in the decomposition

of NH_4F is likely to etch the glass parts in the reactor or the substrate holder made of quartz. The volatile etching products, namely SiF_x, are expected to be the origin of the Si impurities detected in the films. To investigate whether Si incorporation is occurring also in the current process, a special film stack was deposited and measured with ToF-ERDA. The film stack consists of a Si substrate, a ~90 nm GdF_3 film deposited at 325 °C, and a ~90 nm Ta_2O_5 film deposited at 300 °C. The role of the Ta_2O_5 film is to prevent the fast erosion of the GdF_3 film during the measurement. The depth profile of the film stack is therefore more accurate, and the separation between Si signals originating from the film and the substrate is possible. According to ToF-ERDA, Si impurities are present, at least in the film deposited at 325 °C. However, the Si content is only 0.19 ± 0.04 at-%. It should be noted, that besides some Si incorporation in the films, some visual changes due to HF exposure were noticed in the precursor source tubes made of glass. Nevertheless, no other effects on the appearance or performance of reactor components or vacuum pump were observed.

The morphology of the films was investigated with FESEM. Fig. 5 presents FESEM images of approximately 100 nm thick films deposited at 300–375 °C. All the films are clearly polycrystalline and a clear trend is seen in the morphology. The higher the deposition temperature, the more uniform the films appear. In the film deposited at the lowest temperature, distinct grains are pointing out of the surface while the surface is otherwise smooth. As the deposition temperature is increased, the films become more homogeneous. In the film deposited at the highest temperature, the surface is homogeneous, yet seemingly rougher than in the films deposited at lower temperatures.

The morphology was studied also for a thinner 26 nm film deposited at 300 °C. As seen in Fig. 6a, the upward pointing structures are not yet seen in this film. In addition to the Si substrates, deposition was tested also on sapphire substrates. The main motivation for using sapphire substrates came from UV-Vis transmittance studies that will be discussed later. Fig. 6 b shows a FESEM image of a 1600 cycle (35 nm) film deposited on sapphire at 300 °C. The morphology of the film is similar to the 100 nm films deposited on Si at the same temperature. Also the GPC values on the two substrates are similar.

FIG. 5. FESEM images of approximately 100 nm thick films deposited on silicon substrate at 300–375 °C.

FIG. 6. FESEM images of GdF_3 films deposited at 300 °C on a) silicon (26 nm film) and b) sapphire (35 nm film).

AFM images confirm the trend in the morphology on Si substrates. Figure 7. shows the images of approximately 100 nm thick films deposited at 300–375 °C. The upward pointing grains are clearly seen in the film deposited at 300 °C, whereas the surface of the film deposited at 375 °C is the most homogeneous. The lowest roughness is measured from the film deposited at 350 °C. At that temperature, the upward pointing

grains have almost completely vanished, but the surface roughening related to grain growth at high deposition temperature is not yet seen. The root mean square roughness (R_q) values for the films deposited at 300, 325, 350, and 375 °C are 9.5, 6.5, 6.3, and 8.1 nm, respectively.

FIG. 7. AFM images and calculated roughness in R_q of approximately 100 nm films deposited at a) 300, b) 325, c) 350, and d) 375 °C.

The densities of the films deposited at 285–375 °C, were evaluated from XRR curves. For approximately 25 nm thick films, the densities are 6.80–6.95 g/cm^3, and close to the density 7.06 g/cm^3 calculated from the unit cell parameters.[35] The refractive indices of the same films as measured by ellipsometry at a wavelength of 633 nm are 1.50–1.51. In the literature, refractive indices between 1.56–1.57 have been reported.[37]

To estimate the antireflection properties of the films, UV-Vis spectra were measured in the wavelength range of 190−1100 nm. Sapphire was used as a substrate, because it is transparent up to high photon energies. Figure 8. depicts the spectra of a 35 nm GdF_3 film deposited on a sapphire substrate at 300 °C and a bare sapphire substrate. It is seen, that the GdF_3 film serves as an antireflection coating on sapphire across the whole wavelength range; the transmittance is higher than without the GdF_3 film.

FIG. 8. UV-Vis spectra for bare sapphire (bolded curve) and GdF_3 deposited on sapphire at 300 °C.

The insulator properties of the films deposited at 300, 325, and 350 °C were studied by making capacitor structures consisting of a GdF_3 film deposited on ITO coated glass substrate and an aluminum electrode. The film deposited at 300 °C is the purest film according to ToF-ERDA, whereas the film deposited at 350 °C is the smoothest one. The permittivity measured for approximately 45 nm film deposited at 300 °C is 8.9 and for a ~64 nm film 9.3. For the film deposited at 325 °C (43 nm) the permittivity is 9.3, and for the film deposited at 350 °C (~50 nm) it is 10.8.

The reason for the larger permittivity of the 350 °C film may be the larger impurity content of the film. 350 °C is also the temperature where decomposition of $Gd(thd)_3$ is expected. The stoichiometry of the film also deviates from the two other films. F/Gd ratio of 2.7 was measured for the film deposited at 350 °C, whereas F/Gd ratios of 3.3 and 3.2 were obtained for the films deposited at 300 and 325 °C. For other ALD lanthanide fluorides, dielectric constants of 12.3 (LaF_3) and ~6 (YF_3) have been measured.[4, 18]

I-V measurements on samples in the 40–50 nm thickness range were poorly repeatable. The top electrodes were deposited after breaking vacuum, and therefore it is assumed that the films were subjected to surface contamination. Influence of any surface contaminants becomes more pronounced the thinner the dielectric films are. In addition, the influence of surface roughness is likewise stronger in thin layers. For a ca. 64 nm GdF_3 film grown at 300 °C, an I-V curve (Fig. 9) was measured using a long (10 s) measurement delay. The electrons were injected from the ITO side. The material is

clearly an insulator, as expected based on the wide band gap of ~10 eV. While the leakage level at 5 V (corresponding to a 780 kV/cm field) is still low, the material deteriorates quickly when voltages above 5 V are applied. When 6–8 V was applied rapid aging was observed. 9 V was enough to cause dielectric breakdown. When the electrons were injected from the Al side, the devices failed at lower voltages (< 5 V). This observation is in accordance with the assumption that the GdF_3/Al interface may contain more impurities than the ITO/GdF_3 interface. Making strong capacitors with GdF_3 is clearly not as straightforward as with well-established dielectrics such as Al_2O_3 or ZrO_2.

Fig. 9. I-V curve of a 64 nm GdF_3 film deposited on ITO coated glass substrate at 300 °C.

Finally, the adhesion of the films on the Si-substrate was tested with the Scotch tape test. The tested films were 100 nm thick and remained intact according to visual inspection. The films were stable in ambient air. After several months of storage in air their appearance remained unchanged and no phase changes were observed with XRD.

IV. SUMMARY AND CONCLUSIONS

Gadolinium fluoride thin films were deposited by atomic layer deposition. The films were grown at 275–375 °C using $Gd(thd)_3$ and NH_4F as precursors. The films consist of orthorhombic GdF_3, and the impurity contents of H, C, N and O are low. In contrast to

TiF_4-based ALD metal fluoride processes, the GPC stays nearly constant along the studied temperature range, namely 0.22–0.26 Å at 275–375 C°. The film thickness also grows linearly with applied cycles. The relatively narrow deposition temperature range is limited by increasing amount of impurities at low deposition temperatures and increasing roughness at high deposition temperatures. Although $Gd(thd)_3$ has been reported to decompose at 350 °C, no significant decomposition was observed in this study. The films deposited at 300 °C serve as an antireflective coating in the wavelength range of 190–1100 nm as tested on sapphire substrate. Electrical properties were measured and for example permittivity values of 8.9 and 9.3 were measured for 45 nm and 64 nm films deposited at 300 °C.

ACKNOWLEDGMENTS

The use of ALD center Finland research infrastructure is acknowledged.

DATA AVAILABILITY

The data that support the findings of this study are available from the corresponding author upon reasonable request.

REFERENCES

[1]J. Schlett, Photonics Spectra, **55**, 34 (2021).

[2]L. J. Lingg, J. D. Targove, J. P. Lehan, and H. A. Macleod, Proc. SPIE **818**, 86 (1987).

[3]H. Schink, J. Kolbe, F. Zimmermann, D. Ristau, and H. Welling, Proc. SPIE **1441**, 327 (1991).

[4]T. Pilvi, E. Puukilainen, K. Arstila, M. Leskelä, and M. Ritala, Chem. Vapor Depos. **14**, 85 (2008).

[5]J. Andres and A. Chauvin, The Rare Earth Elements, edited by David A. Atwood (Wiley, Chichester, 2012), pp. 139 and 392–393

[6]Solid State Luminescence, Theory, Materials and Devices, edited by A. H. Kitai (Chapman & Hall, London, 1993), p. 45

[7]S. Gai, C. Li, P. Yang, and J. Lin, Chem. Rev. **114**, 2343 (2014).

[8]X. Qiao, J. Zhou, J. Xiao, Y. Wang, L. Sun, and C. Yan, Nanoscale **4**, 4611 (2012).

[9]W. G. J. H. M. van Sark, J. de Wild, J. K. Rath, A. Meijerink, and R. E. I. Schropp, Nanoscale Res. Lett. **8**, 81 (2013).

[10]M. B. de la Mora, O. Amelines-Sarria, B. M. Monroy, C. D. Hernández-Pérez, and J. E. Lugo, Sol. Energ. Mat. Sol. C. **165**, 59 (2017).

[11]Y. Pan, X. Wei, W. Wang, H. Chen, and Y. Li, Opt. Mater. **107,** 110156 (2020).

[12]P. Kumar, S. Singh, and B. K. Gupta, Nanoscale **8**, 14297 (2016).

[13]H. Xia, L. Lei, W. Hong, and S. Xu, J. Alloy Compd. **757**, 239 (2018).

[14]T. Mahalingam and M. Radhakrishnan, J. Mater. Sci. Lett. **6**, 1135 (1987).

[15] E. Rogers, P. Dorenbos, E. Van Der Kolk, New J. Phys. **13**, 093038 (2011).

[16]G. Malandrino, O. Incontro, F. Castelli, I. L. Fragalà, and C. Benelli, Chem. Mater. **8**, 1292 (1996).

[17]M. Leskelä and M. Ritala, Thin Solid Films **409**, 138 (2002).

[18]T. Pilvi, E. Puukilainen, F. Munnik, M. Leskelä, and M. Ritala, Chem. Vapor Depos. **15**, 27 (2009).

[19]E. Atosuo, J. Ojala, M. J. Heikkilä, M. Mattinen, K. Mizohata, J. Räisänen, M. Leskelä, and M. Ritala. J. Vac. Sci. Technol**.** A **39**, 022404 (2021).

[20]T. Pilvi, K. Arstila, M. Leskelä, and M. Ritala, Chem. Mater. **19**, 3387 (2007).

[21]T. Pilvi, T. Hatanpää, E. Puukilainen, K. Arstila, M. Bischoff, U. Kaiser, N. Kaiser, M. Leskelä, and M. Ritala, J. Mater. Chem. **17**, 5077 (2007).

[22]T. Pilvi, E. Puukilainen, U. Kreissig, M. Leskelä, and M. Ritala, Chem. Mater. **20**, 5023 (2008).

[23]M. Mäntymäki, J. Hämäläinen, E. Puukilainen, F. Munnik, M. Ritala, and M. Leskelä, Chem. Vapor Depos. **19**, 111 (2013).

[24]M. Mäntymäki, J. Hämäläinen, E. Puukilainen, T. Sajavaara, M. Ritala, and M. Leskelä, Chem. Mater. **25**, 1656 (2013).

[25]M. Mäntymäki, M. J. Heikkilä, E. Puukilainen, K. Mizohata, B. Marchand, J. Räisänen, M. Ritala, and M. Leskelä, Chem. Mater. **27**, 604 (2015).

[26]M. Mäntymäki, K. Mizohata, M. J. Heikkilä, J. Räisänen, M. Ritala, and M. Leskelä, Thin Solid Films **636**, 26 (2017).

[27]D. H. K. Jackson, M. R. Laskar, S. Fang, S. Xu, R. G. Ellis, X. Li, M. Dreibelbis, S. E. Babcock, M. K. Mahanthappa, D. Morgan, R. J. Hamers, and T. F. Kuech, J. Vac. Sci. Technol**.** A **34**, 031503 (2016).

[28]O. Tiurin, N. Solomatin, M. Auinat, and Y. Ein-Eli, J. Power Sources **448**, 227373 (2020).

[29]J. Xie, A. D. Sendek, E. D. Cubuk, X. Zhang, Z. Lu, Y. Gong, T. Wu, F. Shi, W. Liu, E. J. Reed, and Y. Cui, ACS Nano **11**, 7019 (2017).

[30]M. Ylilammi and T. Ranta-aho, J. Electrochem. Soc. **141**, 1278 (1994).

[31]J. N. Kvalvik, K. B. Kvamme, K. Almaas, A. Ruud, H. H. Sønsteby, and O. Nilsen, J. Vac. Sci. Technol**.** A **38,** 050401 (2020).

[32]PA. Hansen, T. Zikmund, T. Yu, J. N. Kvalvik, T. Aarholt, Ø. Prytz, A. Meijerink, and O. Nilsen, Commun. Chem. **3**, 162 (2020).

[33]M. Ylilammi and T. Ranta-aho, Thin Solid Films **232**, 56 (1993).

[34]J. Niinistö, N. Petrova, M. Putkonen, L. Niinistö, K. Arstila, and T. Sajavaara, J. Cryst. Growth **285**, 191 (2005).

[35]PDF 12-0788, JCPDS-ICDD, International Center for Diffraction Data

[36]PDF 12-0797, JCPDS-ICDD, International Center for Diffraction Data

[37]R. Thielsch, J. Heber, H. Uhlig, and N. Kaiser, Proc. SPIE **5963**, 59630O (2005).

Journal of Vacuum Science Technology A

PLEASE CITE THIS ARTICLE AS DOI: 10.1116/6.0001629

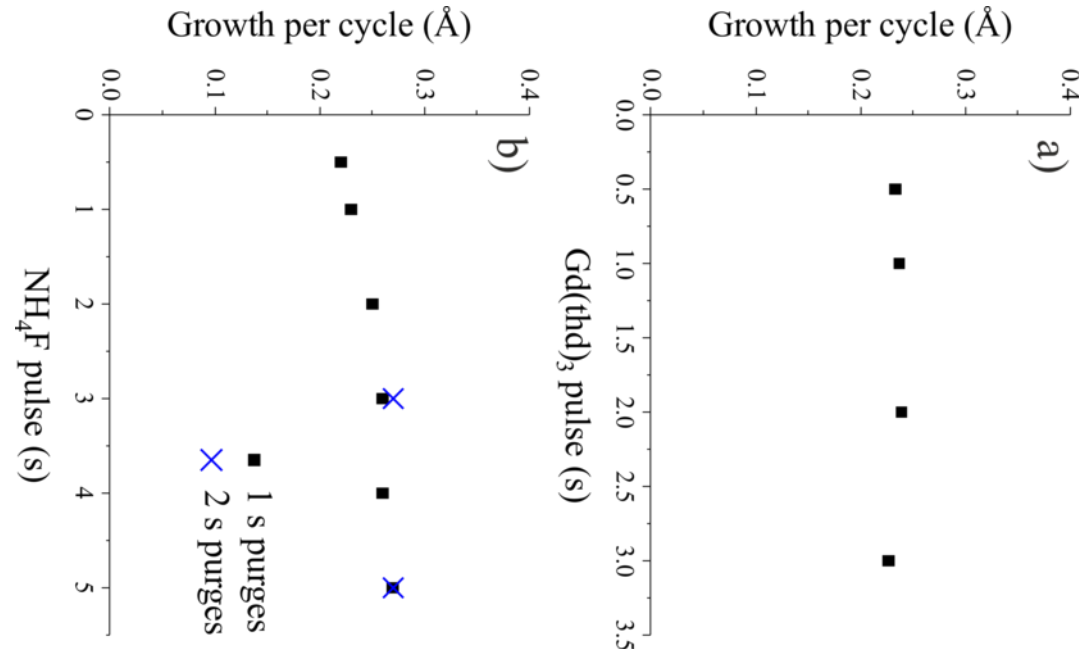

Journal of Vacuum Science Technology A

PLEASE CITE THIS ARTICLE AS DOI: 10.1116/6.0001629

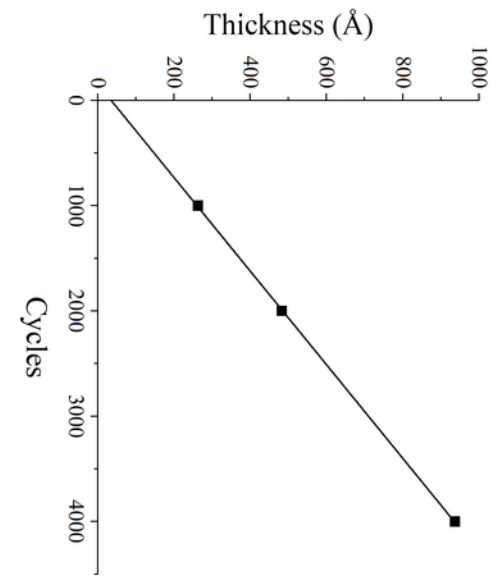

Journal of Vacuum Science Technology A

PLEASE CITE THIS ARTICLE AS DOI: 10.1116/6.0001629

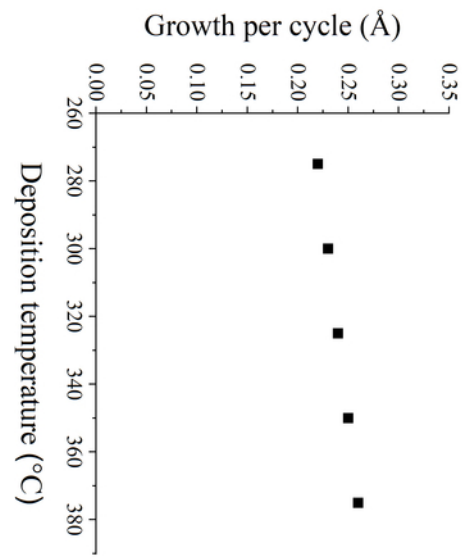

Journal of Vacuum Science Technology A

PLEASE CITE THIS ARTICLE AS DOI: 10.1116/6.0001629

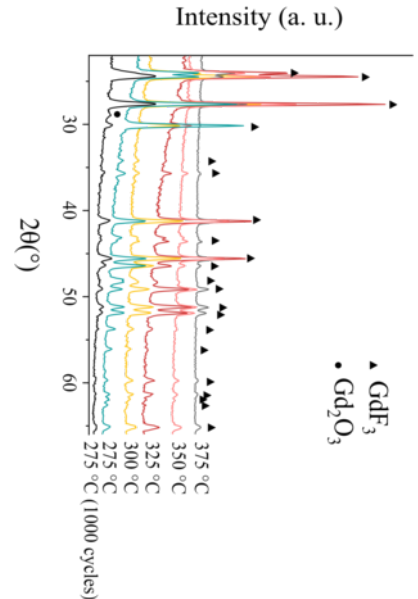

Journal of Vacuum Science Technology A

PLEASE CITE THIS ARTICLE AS DOI: 10.1116/6.0001629

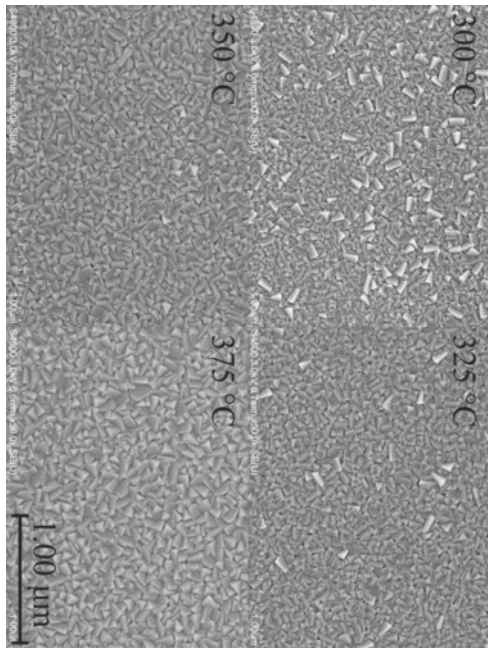

Journal of Vacuum Science Technology A

PLEASE CITE THIS ARTICLE AS DOI: 10.1116/6.0001629

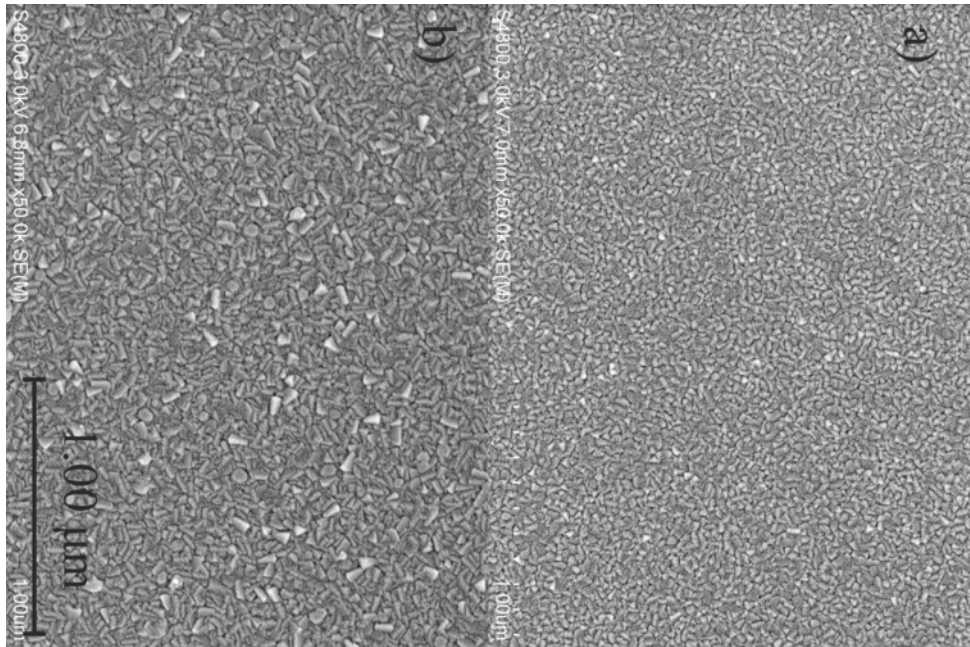

Journal of Vacuum Science Technology A

Journal of Vacuum Science Technology A

PLEASE CITE THIS ARTICLE AS DOI: 10.1116/6.0001629

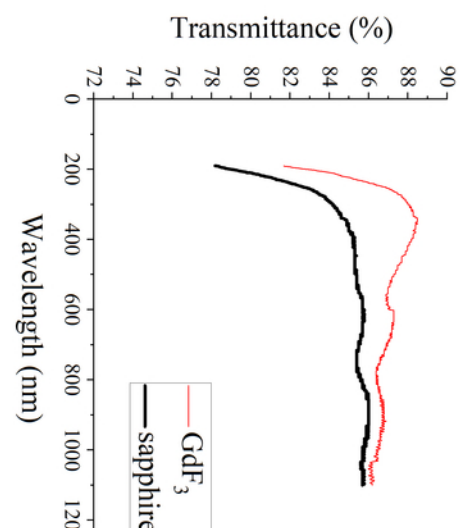

Journal of Vacuum Science Technology A

PLEASE CITE THIS ARTICLE AS DOI: 10.1116/6.0001629